Improved Buffer-Aided Selective Relaying for Free Space Optical Cooperative Communications

Chadi Abou-Rjeily, *Senior Member IEEE*

***Abstract*—This paper tackles the performance analysis and relaying strategies for two-relays buffer-aided (BA) parallel relaying cooperative free space optical (FSO) networks. We first provide an asymptotic analysis of the existing selective relaying scheme that simultaneously activates the strongest source-relay (S-R) and relay-destination (R-D) optical links. We then propose an improvement of this scheme and highlight on its advantages by deriving closed-form accurate expressions for the asymptotic values of the outage probability (OP) and average packet delay (APD). The theoretical evaluation and numerical analysis demonstrate the capability of the improved scheme in enhancing the diversity order with finite buffer sizes unlike the selective relaying scheme that achieves diversity gains only with infinite-size buffers entailing infinite delays. The OP performance is significantly enhanced for all network topologies whether the relays are closer to S, closer to D or placed at the same distance from S and D. On the other hand, the reaped APD gains depend on the positions of the relays.**

***Index Terms*—Free-Space Optics, FSO, relaying, Markov chain, outage probability, queuing delay, asymptotic analysis, cooperative networks.**

I. Introduction

Free Space Optics (FSO) emerged as a mature technology for realising license-free, secure and high speed outdoor optical wireless communications [1]. In order to mitigate the limiting effects of turbulence-induced scintillation, relaying strategies were extensively studied in the context of FSO communications. The decode-and-forward (DF) FSO relaying techniques evolved from the buffer-free (BF) solutions [2], [3] to buffer-aided (BA) solutions where the relays are equipped with buffers in which the incoming packets can be temporarily stored until the channel conditions are more favorable [4]–[7]. For delay-tolerant applications, this additional degree of freedom can remarkably improve the reliability of the cooperative network at the expense of introducing queuing delays.

The literature on BA relaying for radio frequency (RF) communications is extensive and the relaying protocols revolve mainly around the selection of a single half-duplex (HD) relay to either transmit or receive within each time slot [8]–[14]. Relay selection can be based solely on the channel state information (CSI) [8], [9] or can include the buffer state information (BSI) in the selection process [10]–[14]. While the former approach is simpler, the latter approach achieves enhanced performance levels at the expense of an increased complexity since the actual numbers of packets stored in all relays' buffers must be known. In fact, this knowledge can be exploited for balancing the load among the relays' buffer resulting in a more efficient flow of the data packets between the source and the destination [10]–[14]. In [15], BA relaying was considered with a single full-duplex (FD) RF relay having an infinite buffer size. An additional state pertaining to the relay concurrently receiving and transmitting was included with the objective of maximizing the throughput for a communication session that extends over an infinite number of time slots. Similarly, BA FD multi-hop relaying was studied in [16]. While [8]–[14] considered BA DF parallel relaying, BA DF serial relaying was studied in [17] and BA amplify-and-forward (AF) parallel relaying was considered in [18]; all in the context of HD relaying. Finally, the impact of the direct source-destination link was analyzed in [19] in the context of BA DF parallel relaying with HD relays. [8]–[19] tackled the problem of slot-by-slot BA relaying where the decision on the link to be activated is made within each time slot. On the other hand, [20] considered the problem of BA relaying with the objective of maximizing the network throughput for a communication session that extends over an infinite number of time slots. Hybrid RF/FSO relaying was considered with infinite-size buffers [20].

FSO relays operate naturally in the FD mode since unique opto-electronic components are deployed at the receiving photo-detector front end and at the transmitting laser. Moreover, FSO networks are interference-free following from the high directivity of the FSO links unlike the broadcast nature of RF transmissions. These unique features of the FSO networks were exploited in [4] for proposing a novel selective relaying (SR) protocol that is based on the simultaneous activation of the strongest source-relay link and the strongest relay-destination link. The concurrent transmissions along the two hops resulted in reduced outages and delays compared to the *max-link* HD scheme in [8] that is based on the activation of a single link in each time slot. While parallel relaying was considered in [4], serial relaying FSO BA networks were studied in [5]. The SR scheme in [4] and the multi-hop scheme in [5] were based on the CSI where the BSI was limited to avoiding the reception (resp. transmission) at full (resp. empty) buffers. While fixed relays were considered in [4], [5], moving relays in the form of FSO unmanned aerial vehicles (UAVs) were studied in [6] which offered the capability of adapting the hovering position of the UAV to the atmospheric conditions. While one type of traffic was considered in [4]–[6], the FSO relaying scheme in [7] tackled two types of traffic; namely, a low priority delay-tolerant traffic and a high priority non-delay-tolerant traffic with the objective of guaranteeing the

The author is with the Department of Electrical and Computer Engineering of the Lebanese American University (LAU), PO box 36 Byblos 961, Lebanon. (e-mail: chadi.abourjeily@lau.edu.lb).

best quality-of-service (QoS) to the latter type of traffic. BA relaying was also considered with mixed and hybrid RF/FSO networks where the relay is equipped with a buffer for storing the packets from the mobile RF users before multiplexing the generated traffic over the backhaul FSO link [21]–[23]. While a single infinite-size buffer was considered in [21], [22], the work in [23] revolved around the deployment of multiple finite-size buffers with different packet unloading strategies for the sake of achieving a QoS differentiation among the RF users. BA parallel relaying hybrid RF/FSO backhaul networks were studied in [24] where an adaptive transmission scheme was adopted with simultaneous transmissions along the FSO and RF links.

This paper targets an improvement of the existing BA FSO SR scheme in [4]. The proposed improved SR (ISR) strategy prioritizes the simultaneous reception and transmission from the same FD relay which positively impacts the outage probability (OP) and average packet delay (APD). Similar to the SR scheme, the proposed ISR scheme is based solely on the CSI without the need of acquiring the states of the buffers which positively impacts the ease of implementation. The performances of the SR and ISR schemes are analyzed based on a Markov chain (MC) framework in the case of two relays driven by the fact that the number of states of the MC increases exponentially with the number of relays rendering the theoretical analysis out of reach in the general case of an arbitrary number of relays. Finally, by identifying the most probable states of the MC, we derive closed-form OP and APD asymptotic expressions for the SR and ISR schemes. The simplicity of the derived asymptotic expressions allows to draw conclusions on the limitations of the SR scheme and on the significant performance gains that can be reaped from the ISR scheme especially with finite-size buffers. As such, the contributions of this work are three-fold:

- For cooperative networks with two relays, we present a theoretical performance analysis of the existing SR scheme and we derive closed-form expressions of the asymptotic OP and APD. The novel results identified major weaknesses in the state-of-the-art SR scheme that suffers from an inherent tradeoff between OP and APD. This scheme reaps the diversity gains only with impractical infinite-size buffers at the expense of incurring unbounded delays. This type of analysis and the drawn results were not previously presented in [4].
- We propose a novel relaying strategy for BA FSO communications. This CSI-based scheme is appealing because of its ease-of-implementation and performance gains. The presented analysis demonstrates that this novel scheme is capable of achieving significant OP and APD gains while requiring limited signaling overhead and deploying practical finite-size buffers of size two.
- Through a MC framework, we evaluate the analytical performance of the proposed scheme followed by an asymptotic analysis to quantify the asymptotic OP and APD performance with two relays. While the MC framework constitutes the broad mathematical tool to analyze queues [4], [5], [7], [8], [10]–[13], the particularities of the underlying network and the implemented relaying strategy render the MC analysis different from one system to another.

FSO communications are either applied as a parallel backup to other RF or mmWave systems, or built separately as an independent entity. One possible application of the proposed system is in the 5G backhaul framework [25] where the small cell base stations define the source, destination and relays nodes. Backhaul systems are characterized by data-intensive transmissions and small cell base stations can be equipped with FSO transceivers to relay the backhaul traffic in a reliable and efficient manner. Furthermore, UAV-based FSO communications are widely investigated because of the ability of UAVs to adjust their positions dynamically to establish LoS links [26]. The parallelism proposed in this model will increase the diversity order of such systems which makes the communications more reliable. BA relaying can also enhance the secrecy rate of networks with eavesdroppers. In this scenario, buffers will add extra degrees of freedom that increase the number of links that can be selected and hence increase the possibility of avoiding transmitting along links that are prone to eavesdropping [27].

The remainder of the paper is organized as follows. The system model, BA relaying and MC framework are presented in Section II. The performance analysis of the SR scheme is provided in Section III. The novel BA FSO relaying scheme is presented in Section IV along with an asymptotic analysis for different network setups. Simulations over gamma-gamma fading channels with pointing errors are presented in Section V. Finally, Section VI concludes the paper.

II. System Model

A. Basic Parameters

Consider an intensity-modulated with direct-detection (IM/DD) FSO system where the source (S) communicates with the destination (D) through two parallel DF relays (R's). We assume that the direct link between S and D is unavailable because of the excessive distance between these nodes or the presence of an obstacle, for example. A quasi-symmetrical network topology is assumed where both relays are placed at a distance d_1 from S and at a distance d_2 from D. The system model is depicted in Fig. 1.

We consider a FSO channel model that takes into account the combined effects of path loss, atmospheric turbulence-induced scintillation and misalignment-induced fading caused by pointing errors [28]. A FSO link is defined to be in outage if the instantaneous signal-to-noise ratio (SNR) along this link falls below a detection threshold SNR required to achieve a given target rate [8]. Denoting by $\mathfrak{p}_1$ and $\mathfrak{p}_2$ the outage probabilities along the S-R and R-D links, respectively, these outage probabilities can be determined from the following expression in the case of background noise limited receivers corrupted by additive white Gaussian noise [5]:

$$\mathfrak{p}_n = \frac{\xi_n^2}{\Gamma(\alpha_n)\Gamma(\beta_n)} G_{2,4}^{3,1}\left[\frac{\alpha_n\beta_n}{G_n(P_M/2)}\middle|\begin{matrix}1, \xi_n^2+1\\ \xi_n^2, \alpha_n, \beta_n, 0\end{matrix}\right], \quad (1)$$

where $G_{p,q}^{m,n}[\cdot]$ is the Meijer G-function and $\Gamma(\cdot)$ is the gamma function. In this paper, the performance metrics of

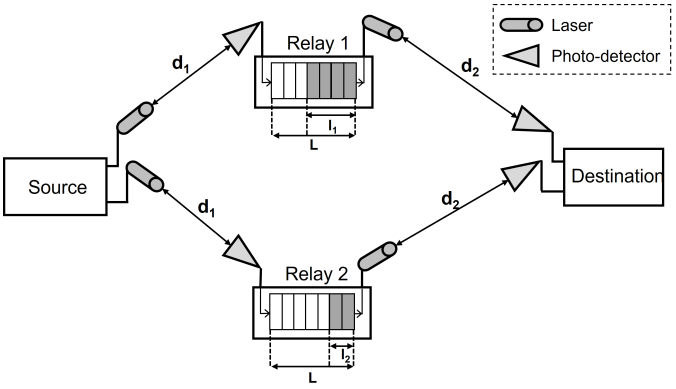

Fig. 1. System model of a BA FSO communication system.

the cooperative network will be determined as a function of the parameter $P_M \triangleq \frac{\eta}{\sqrt{\gamma_{\text{th}} N_0}}$ that denotes the optical power margin of the average SNR with respect to the threshold SNR γ_{th} where η and N_0 denote the optical-to-electrical conversion ratio and the power of the Gaussian noise, respectively [4]. The power margin P_M is normalized by the factor of 2 in (1) following from evenly splitting the optical power among the S-R and R-D hops for the sake of a fair comparison with point-to-point single-hop FSO communication systems.

In (1), α_n and β_n stand for the parameters of the gamma-gamma distribution of the atmospheric scintillation:

$$\alpha_n = \left[\exp\left(0.49\sigma_{R,n}^2/(1+1.11\sigma_{R,n}^{12/5})^{7/6}\right) - 1\right]^{-1} \quad (2)$$

$$\beta_n = \left[\exp\left(0.51\sigma_{R,n}^2/(1+0.69\sigma_{R,n}^{12/5})^{5/6}\right) - 1\right]^{-1}, \quad (3)$$

where $\sigma_{R,n}^2 = 1.23 C_n^2 k^{7/6} d_n^{11/6}$ is the Rytov variance where k is the wave number and C_n^2 denotes the refractive index structure parameter. In (1), the parameter ξ_n is related to the pointing errors [28]:

$$\xi_n = 2^{-\frac{5}{4}} \frac{\omega_{z,n}}{\sigma_{s,n}} \sqrt{\frac{\omega_{z,n}}{a_n}} \text{erf}^{\frac{1}{2}}\left(\sqrt{\frac{\pi}{2}} \frac{a_n}{\omega_{z,n}}\right) e^{\frac{\pi}{4}\frac{a_n^2}{\omega_{z,n}^2}}, \quad (4)$$

where $\text{erf}(\cdot)$ is the error function while $\omega_{z,n}$, a_n and $\sigma_{s,n}$ stand for the beam waist, receiver radius and pointing error displacement standard deviation along the n-th hop, respectively.

In (1), G_n is a gain factor that follows since the n-th hop is shorter than the direct link S-D:

$$G_n = e^{-\sigma(d_n - d_{\text{SD}})} \frac{A_n}{A_{\text{SD}}} \frac{\xi_{\text{SD}}^2 + 1}{\xi_{\text{SD}}^2}, \quad (5)$$

where σ is the attenuation coefficient and d_{SD} is the distance between S and D. Finally, $A_n = \text{erf}^2\left(\sqrt{\frac{\pi}{2}} \frac{a_n}{\omega_{z,n}}\right)$ while A_{SD} and ξ_{SD} are the pointing error parameters of the link S-D.

For $P_M \gg 1$, the outage probability in (1) scales asymptotically as $P_M^{-\min\{\beta_n, \xi_n^2\}}$ [5] implying a diversity order of $\delta_n \triangleq \min\{\beta_n, \xi_n^2\}$ along the links of the n-th hop. In what follows, we denote $p \triangleq \mathfrak{p}_1$ and $q \triangleq \mathfrak{p}_2$ for the sake of notational simplicity.

B. Buffer-Aided Relaying

In this work, buffer-aided (BA) DF relaying is considered where each one of the two relays is equipped with a buffer of finite size L in which the information packets from S can be temporarily stored until the channel conditions are more favorable. The source is assumed to be equipped with an infinite size buffer and to be fully backlogged; i.e. it always has enough information to transmit [4]–[6], [8], [10], [15]. We denote by l_k (with $0 \leq l_k \leq L$) the actual number of packets stored in the buffer of relay R_k for $k = 1, 2$.

Since an incoming packet cannot be accommodated in a full buffer, then R_k must be refrained from receiving if $l_k = L$. Similarly, R_k must be refrained from transmitting when its buffer is empty; i.e. $l_k = 0$. As such, we define the sets of relays (along with their cardinalities) as follows [4]:

$$\mathcal{C}_r \triangleq \{k = 1, 2 \mid l_k \neq L\} \;\; ; \;\; |\mathcal{C}_r| \triangleq \phi_{l_1,l_2}, \quad (6)$$

$$\mathcal{C}_t \triangleq \{k = 1, 2 \mid l_k \neq 0\} \;\; ; \;\; |\mathcal{C}_t| \triangleq \psi_{l_1,l_2}, \quad (7)$$

$$\mathcal{C}_{r,t} \triangleq \{k = 1, 2 \mid l_k \neq L \;\&\; l_k \neq 0\} \;\; ; \;\; |\mathcal{C}_{r,t}| \triangleq \theta_{l_1,l_2}, \quad (8)$$

denoting the relays that can receive, transmit and both receive and transmit, respectively. Note that the cardinalities of the sets $\mathcal{C}_r$, $\mathcal{C}_t$ and $\mathcal{C}_{r,t}$ depend on the values taken by (l_1, l_2) and these cardinalities are denoted by ϕ_{l_1,l_2}, ψ_{l_1,l_2} and θ_{l_1,l_2}, respectively.

If $L = 1$, then $l_k \in \{0, \ldots, L\} = \{0, 1\}$ implying that either the link R_k-D is unavailable if $l_k = 0$ (empty buffer) or the link S-R_k is unavailable if $l_k = 1$ (full buffer). As such, at any time instance, two out of the four links in the network are always unavailable which negatively impacts the reliability of the system. Therefore, in what follows, we assume that $L \geq 2$.

The signaling information has to be shared with a central node that makes a decision on the links to be activated in a given time slot. This role can be played by the source node S, for example. This node informs each relay of its role (i.e. receive, transmit or simultaneously receive and transmit) by the exchange of short 2-bit messages.

C. Markov Chain Framework and Performance Metrics

A Markov chain (MC) analysis will be adopted for evaluating the performance of the BA relaying system. A state of the discrete-time discrete-value MC is represented by the numbers of packets present in the relays' buffers $(l_1, l_2) \in \{0, \ldots, L\}^2$ resulting in a total of $N_s \triangleq (L+1)^2$ possible states. We denote by $t_{(l_1,l_2),(l_1',l_2')}$ the transition probability of the MC evolving from the state (l_1, l_2) at a certain time slot to the state (l_1', l_2') in the subsequent slot. The transition probabilities satisfy the following relation:

$$\sum_{l_1'=0}^{L} \sum_{l_2'=0}^{L} t_{(l_1,l_2),(l_1',l_2')} = 1 \;\; \forall \;\; (l_1, l_2) \in \{0, \ldots, L\}^2. \quad (9)$$

The transition probabilities can be stacked in the $N_s \times N_s$ state transition matrix $\mathbf{T}$ that can be used to evaluate the steady-state probability distribution as follows [4], [8]:

$$\mathbf{\Pi} = (\mathbf{T} - \mathbf{I} + \mathbf{B})^{-1} \mathbf{b}, \quad (10)$$

where $\mathbf{I}$ and $\mathbf{B}$ are $N_s \times N_s$ matrices denoting the identity matrix and all-one matrix, respectively. Vector $\mathbf{b}$ is the N_s-dimensional vector whose elements are all equal to 1. The N_s-dimensional vector $\mathbf{\Pi}$ can be written as $\mathbf{\Pi} = [\pi_{0,0}, \ldots, \pi_{0,L}, \ldots, \pi_{L,0}, \ldots, \pi_{L,L}]^T$ where π_{l_1,l_2} stands for the probability of having l_1 packets stored in the buffer of R_1 and l_2 packets stored in the buffer of R_2 at steady-state with $\sum_{l_1=0}^{L}\sum_{l_2=0}^{L}\pi_{l_1,l_2} = 1$.

The steady-state distribution is useful for deriving the outage probability (OP) and average packet delay (APD) of the BA network. The cooperative network is in outage if no packets can be communicated along any of the four constituent links S-R_1, S-R_2, R_1-D and R_2-D resulting in the following expression of the OP [4]:

$$P_{out} = \sum_{l_1=0}^{L}\sum_{l_2=0}^{L}\pi_{l_1,l_2}p^{\phi_{l_1,l_2}}q^{\psi_{l_1,l_2}}, \tag{11}$$

since ϕ_{l_1,l_2} relays can receive and thus the S-R hop is in outage with probability $p^{\phi_{l_1,l_2}}$ while ψ_{l_1,l_2} relays can transmit implying that the R-D hop is in outage with probability $q^{\psi_{l_1,l_2}}$ where ϕ_{l_1,l_2} and ψ_{l_1,l_2} are defined in (6)-(7).

From [4], the APD accounting for the queuing delays accumulated at the buffers of S and the relays can be determined from the following relation that results from Little's law [29]:

$$APD = \frac{\bar{L}}{\eta_s} + \frac{1}{\eta_s} - 1, \tag{12}$$

where the APD is expressed in terms of the normalized time unit that is equal to the duration of one information packet. In (12), $\bar{L}$ denotes the average queue length corresponding to the average number of packets stored in the relays' buffers:

$$\bar{L} = \sum_{l_1=0}^{L}\sum_{l_2=0}^{L}\pi_{l_1,l_2}(l_1+l_2), \tag{13}$$

while η_s stands for the input throughput at the relays:

$$\eta_s = \sum_{l_1=0}^{L}\sum_{l_2=0}^{L}\pi_{l_1,l_2}\left(1-p^{\phi_{l_1,l_2}}\right). \tag{14}$$

III. Selective Relaying (SR)

The selective relaying (SR) protocol proposed in [4] is based on the simultaneous activation of the strongest S-R link and the strongest R-D link. The transition probabilities of the SR scheme were derived in [4] as follows:

$$t_{(l_1,l_2),(l_1,l_2)} = p^{\phi}q^{\psi} + \frac{\theta}{\phi\psi}(1-p^{\phi})(1-q^{\psi}), \tag{15}$$

$$t_{(l_1,l_2),(l_1+1,l_2)} = t_{(l_1,l_2),(l_1,l_2+1)} = \frac{1}{\phi}(1-p^{\phi})q^{\psi}, \tag{16}$$

$$t_{(l_1,l_2),(l_1-1,l_2)} = t_{(l_1,l_2),(l_1,l_2-1)} = \frac{1}{\psi}(1-q^{\psi})p^{\phi}, \tag{17}$$

$$t_{(l_1,l_2),(l_1+1,l_2-1)} = t_{(l_1,l_2),(l_1-1,l_2+1)} = \frac{1}{\phi\psi}(1-p^{\phi})(1-q^{\psi}), \tag{18}$$

where the subscripts of ϕ, ψ and θ were dropped for simplicity.

The transition probabilities in (15)-(18) were derived in [4] and used to derive the steady-state distribution according to (10) and, subsequently, the OP and APD from (11) and (12), respectively. However, the theoretical evaluation was not pursued for deriving closed-form expressions that relate the OP and APD to the network parameters p, q and L in an insightful manner. In fact, the closed-form evaluation was hindered primarily by the large number of states and by the matrix inversion in (10) that involves a $N_s \times N_s$ matrix whose dimensions increase exponentially with the buffer size L.

As such, in this paper, we take the performance analysis one step further by deriving closed-form approximate expressions of the OP and APD that are highly accurate in the asymptotic regime. As will be highlighted later, significant conclusions can be drawn from the aforementioned simple expressions.

Proposition *1 (New Result):* For $P_M \gg 1$, the dominant states; i.e. the states with the highest steady-state probabilities, are confined in the set:

$$\mathcal{S} = \{(l_1,l_2) \mid l_1+l_2 \in \{L-1, L, L+1\}\}, \tag{19}$$

while the steady-state probabilities of the remaining states tend to zero asymptotically.

The asymptotic values of the steady-state probabilities are given by:

$$\pi_{l,L-1-l} = \begin{cases} \mu_1, & l=0 \text{ or } l=L-1; \\ 2\mu_1, & l\neq 0 \text{ and } l\neq L-1. \end{cases} \tag{20}$$

$$\pi_{l,L-l} = \begin{cases} \mu_2, & l=0 \text{ or } l=L; \\ 4\mu_2, & l\neq 0 \text{ and } l\neq L. \end{cases} \tag{21}$$

$$\pi_{l,L+1-l} = \begin{cases} \mu_3, & l=1 \text{ or } l=L; \\ 2\mu_3, & l\neq 1 \text{ and } l\neq L. \end{cases}, \tag{22}$$

where:

$$\begin{cases} \mu_1=\mu_2=\mu_3=\frac{1}{8L-6}, & p=q; \\ \mu_2=\frac{1/2}{(2L-1)+\frac{p}{q}(L-1)}, \mu_1=\frac{p}{q}\mu_2, \mu_3=0, & p>q; \\ \mu_2=\frac{1/2}{(2L-1)+\frac{q}{p}(L-1)}, \mu_3=\frac{q}{p}\mu_2, \mu_1=0, & p<q. \end{cases}. \tag{23}$$

Proof: The proof is based on showing that the set $\mathcal{S}$ in (19) is closed where the probability of exiting $\mathcal{S}$ tends to zero asymptotically. As such, instead of solving the exact balance equations in the entire state space, (20)-(23) can be reached by solving the approximate balance equations in $\mathcal{S}$ since the MC is within this subset of states with a probability that tends to one. The detailed proof is provided in Appendix A. ■

Replacing (20)-(22) in (11) while limiting the summation over the elements of the closed-subset $\mathcal{S}$ results in:

$$P_{out} = 2\mu_2 pq + 2\mu_1 p^2 q + 2\mu_3 pq^2 + \left[2\mu_1(L-2) + 4\mu_2(L-1) + 2\mu_3(L-2)\right]p^2q^2. \tag{24}$$

Replacing (23) in (24) results in the following expressions of the asymptotic OP:

$$P_{out} = \frac{1}{4L-3}\left[pq + p^2q + pq^2 + (4L-6)p^2q^2\right] \;;\; p=q,$$

$$P_{out} = \frac{1}{(2L-1)+\frac{p_{\max}}{p_{\min}}(L-1)}\times \left[pq + p_{\max}^3 + (L-2)p_{\max}^3 p_{\min} + 2(L-1)p^2q^2\right] \;;\; p\neq q, \tag{25}$$

where $p_{\max} \triangleq \max\{p,q\}$ and $p_{\min} \triangleq \min\{p,q\}$.

Replacing (20)-(22) in (13) results in:

$$\bar{L} = [2\mu_1 + 2\mu_1(L-2)](L-1) + [2\mu_2 + 4\mu_2(L-1)]L[2\mu_3 + 2\mu_3(L-2)](L+1). \quad (26)$$

Replacing (23) in (26) while observing from (12) that $APD \approx \bar{L}$ since the throughput η_s in (14) tends to 1 asymptotically, the following asymptotic expressions of the APD can be reached:

$$APD = \begin{cases} L, & p = q; \\ L-1, & p > q; \\ L+1, & p < q. \end{cases} . \quad (27)$$

Note that the asymptotic OP and APD expressions in (25) and (27) are novel and were not reported in the previous work that proposed the FSO BA SR scheme [4]. The advantage of the asymptotic analysis that was carried out in this section resides in relating the asymptotic performance of the SR scheme to the parameters L, p and q in a simple closed-form manner. As such, the novel closed-form expressions in (25) and (27) allow to draw intuitive insights on the performance of SR and on the impact of the buffer size and relay placement on the OP and APD. Moreover, (25) yields the diversity order that constitutes the major metric that captures the performance of the fading-mitigating cooperative diversity method. This important diversity order analysis was missing in [4].

The presented asymptotic analysis allows to draw the following conclusions from the novel results in (25) and (27).

- As L increases, the OP in (25) decreases at the expense of increasing the APD in (27).
- For finite values of the buffer size L, the OP expressions in (25) tend to the values $\frac{pq}{4L-3}$ and $\frac{pq}{(2L-1)+\frac{p_{\max}}{p_{\min}}(L-1)}$ since, for $p \ll 1$ and $q \ll 1$, the probability pq is several orders of magnitude bigger than the probabilities p^2q, pq^2, p^2q^2, $p^3_{\max}$ and $p^3_{\max}p_{\min}$. (i): For $p = q$, the OP behaves asymptotically as pq resulting in the diversity order of $\delta_1 + \delta_2$ which is the same as the diversity order achieved by buffer-free systems. (ii): For $p \neq q$, the OP behaves asymptotically as $\frac{pq}{\frac{p_{\max}}{p_{\min}}(L-1)} = \frac{p^2_{\min}}{L-1}$ since the probability $\frac{p_{\max}}{p_{\min}} \to P_M^{\max\{\delta_1,\delta_2\}-\min\{\delta_1,\delta_2\}} \gg 1$. As such, the achievable diversity order is $2\max\{\delta_1,\delta_2\}$ which is slightly improved with respect to the diversity order $2\min\{\delta_1,\delta_2\}$ of buffer-free systems.
- For $L \to \infty$, the asymptotic OP in (25) tends to $\lim_{L\to+\infty} \frac{4L-6}{4L-3}p^2q^2 = p^2q^2$ for $p = q$. Therefore, for symmetrical networks, the diversity order of the SR scheme is equal to $2\delta_1 + 2\delta_2$ and is double that of the buffer-free systems. On the other hand, for $p \neq q$, (25) tends to $\lim_{L\to+\infty} \frac{L-2}{L-1}\frac{p^3_{\max}p_{\min}}{\frac{p_{\max}}{p_{\min}}}$ since $p^3_{\max}p_{\min} > p^2q^2$. The last expression simplifies to $p^2_{\max}p^2_{\min} = p^2q^2$ implying a diversity order of $2\delta_1 + 2\delta_2$ which significantly exceeds the diversity order $2\min\{\delta_1,\delta_2\}$ of buffer-free systems.

IV. Improved Selective Relaying (ISR)

While the SR scheme selects the strongest S-R and R-D links, the ISR is based on privileging the selection of the available S-R and R-D links that belong to the same relay. In other words, if the links S-R_k and R_k-D (for any $k = 1, 2$) are available, then the ISR strategy selects the relay R_k to carry out the simultaneous reception and transmission. The motivation behind this strategy is that the aforementioned selection ensures the delivery of a packet to D while keeping the numbers of stored packets the same which positively contributes to reducing the delay and enhancing the throughput of the network. As such, this approach contributes to avoiding the congestion (resp. starvation) of the buffer pertaining to the strongest S-R (resp. R-D) link.

The link S-R_k is available only if this link is not in outage and the buffer at R_k is not full so that the incoming packet can be accommodated. Similarly, the link R_k-D is available only if this link is not in outage and the buffer at R_k is not empty so that an information packet can be extracted and transmitted to D. Denoting by P_k and Q_k the unavailability probabilities along the S-R_k and R_k-D links, respectively, these probabilities can be determined as follows:

$$P_k = p + \delta_{l_k=L} - p\delta_{l_k=L} \; ; \; Q_k = q + \delta_{l_k=0} - q\delta_{l_k=0}, \quad (28)$$

where $\delta_s = 1$ if the statement s is true and $\delta_s = 0$ otherwise. In fact, the link S-R_k (resp. R_k-D) is unavailable if either the buffer at R_k is full (resp. empty) or the link is in outage with probability p (resp. q).

An end-to-end link S-R_k-D is available if both its S-R_k and R_k-D hops are available. Consider the following two mutually exclusive events. Event 1: at least one of the links S-R_1-D and S-R_2-D is available. Event 2: none of the links S-R_1-D and S-R_2-D is available. In the case of event 1, the ISR protocol will activate the available end-to-end link (if both end-to-end links are available, a random selection among these links is made). If event 2 describes the state of the network, the ISR protocol will activate the available S-R and R-D links (if any) where these links will not pass through the same relay (since event 1 does not hold). In other words, if the link S-R_k is activated, then the link $R_{\bar{k}}$-D will be activated where $\bar{k} = 2$ if $k = 1$ and $\bar{k} = 1$ if $k = 2$. This clearly distinguishes the proposed ISR protocol from the existing SR scheme that does not differentiate among the aforementioned events in the link selection procedure.

The superiority of ISR over SR is further exhibited through the following example. Consider the scenario where the links S-R_1, S-R_2 and R_1-D are not in outage while the link R_2-D is in outage and assume that the link S-R_2 is stronger than the link S-R_1. Also, assume that none of the buffers is empty or full. In this case, ISR will select R_1 for simultaneous transmission and reception thus ensuring the efficient flow of packets between the terminal nodes S and D. For this relaying protocol, the lengths of the two buffers will remain unchanged. As such, if the above scenario prevails over a number of consecutive time slots, then the ISR selection will not reduce the number of available links in the network since the links S-R_1, S-R_2 and R_1-D will remain available after this transmission epoch. On the other hand, the SR protocol will decide in favor of activating the strongest links S-R_2 and R_1-D (since the link R_1-D that is not in outage is definitely stronger than the link R_2-D that is in outage). Therefore, if this

scenario prevails over a number of consecutive time slots, the buffer at R_2 will keep receiving packets until it becomes full thus rendering the link S-R_2 unavailable since the incoming packets cannot be accommodated. In the same way, R_1 will keep on transmitting packets until its buffer becomes empty thus rendering the link R_1-D unavailable. Consequently, at the end of the transmission epoch, only link S-R_1 will be available implying that the SR selection has entailed the detrimental reduction of the number of available links from three to one. It is worth highlighting that while ISR and SR did not activate the same links in the previous scenario, these protocols might activate the same links in other scenarios. For example, if the links S-R_2 and R_1-D are available while the links S-R_1 and R_2-D are not available, then both protocols will activate the links S-R_2 and R_1-D since these available links will be the strongest links. However, the activation of the same links by ISR and SR for some states of the network does not render ISR a special case of SR.

Denoting by $\mathbf{e}_k$ the k-th row of the 2×2 identity matrix, the transition probabilities of the ISR scheme are (for $k=1,2$):

$$t_{(l_1,l_2),(l_1,l_2)} = P_1P_2Q_1Q_2 + 1-\prod_{k=1}^{2}\left[1-(1-P_k)(1-Q_k)\right] \quad (29)$$

$$t_{(l_1,l_2),(l_1,l_2)+\mathbf{e}_k} = Q_1Q_2(1-P_k)\left[P_{\bar{k}}+\frac{1}{2}(1-P_{\bar{k}})\right] \quad (30)$$

$$t_{(l_1,l_2),(l_1,l_2)-\mathbf{e}_k} = P_1P_2(1-Q_k)\left[Q_{\bar{k}}+\frac{1}{2}(1-Q_{\bar{k}})\right] \quad (31)$$

$$t_{(l_1,l_2),(l_1,l_2)+\mathbf{e}_k-\mathbf{e}_{\bar{k}}} = (1-P_k)P_{\bar{k}}(1-Q_{\bar{k}})Q_k. \quad (32)$$

In (29), a self transition will occur if either all links in the network are unavailable or if at least one the links S-R_1-D and S-R_2-D is available. The complement of the last event is that both links are unavailable where the link S-R_k-D is available only when its two hops S-R_k and R_k-D are available with probability $(1-P_k)(1-Q_k)$. In (30), a packet is transmitted along S-R_k which occurs only if both R-D links are unavailable and the link S-R_k is available. Regarding the other link S-$R_{\bar{k}}$, it can be either unavailable and, if not, a random selection will be made among the two S-R links justifying the factor $1/2$ in (30). A similar justification holds for (31) where a packet is transmitted along R_k-D. In (32), concurrent transmissions take place along the links S-R_k and $R_{\bar{k}}$-D which occurs only if these links are available with probability $(1-P_k)(1-Q_{\bar{k}})$. Regarding the remaining links S-$R_{\bar{k}}$ and R_k-D, these links are both unavailable (with probability $P_{\bar{k}}Q_k$) since, otherwise, an end-to-end S-R-D link will be available and this link will be selected by the ISR scheme. Finally, it can be easily proven that (29)-(32) satisfy (9).

Proposition *2:* Define the set $\mathcal{S}_0$ as:

$$\mathcal{S}_0 = \{(1,1),(0,1),(1,0),(0,2),(2,0)(1,2),(2,1)\}, \quad (33)$$

then, for $P_M \gg 1$ and $p \neq q$, the closed-subset of asymptotically dominant states is given by:

$$\mathcal{S} = \begin{cases} \mathcal{S}_0, & p>q; \\ \{(L-l_1,L-l_2) \mid (l_1,l_2)\in\mathcal{S}_0\}, & p<q. \end{cases} \quad (34)$$

Denoting by $\pi^{(i)}$ the steady-state probability of the i-th element of $\mathcal{S}$, then: $\pi^{(1)}=\nu_1$, $\pi^{(2)}=\pi^{(3)}=\nu_2$, $\pi^{(4)}=\pi^{(5)}=\nu_3$ and $\pi^{(6)}=\pi^{(7)}=\nu_4$ where:

$$\nu_1 = \frac{1}{1+p_{\max}\left(r+\frac{1}{2}\right)} \; ; \; (\nu_2,\nu_3,\nu_4) = \left(\frac{p_{\max}r}{2}, \frac{p_{\max}}{4}, \frac{1}{8r}\right)\nu_1, \quad (35)$$

where $r \triangleq \frac{p_{\max}}{p_{\min}}$.

Proof: The proof is provided in Appendix B. ■

Replacing (33)-(35) in (11) results in:

$$P_{out} = \frac{1}{1+p_{\max}\left(r+\frac{1}{2}\right)}\left[\left(r+\frac{1}{2}\right)p_{\max}^3 p_{\min} + \left(1+\frac{1}{4r}\right)p^2q^2\right]. \quad (36)$$

By observing that $r \gg 1$ and $p_{\max}r \ll 1$ for $P_M \gg 1$, (36) can be further simplified as follows:

$$P_{out} = p_{\max}^4 + p^2q^2 \quad ; \quad p \neq q. \quad (37)$$

Replacing (33)-(35) in (12) results in:

$$APD = \begin{cases} 2, & p>q; \\ 2(L-1), & p<q. \end{cases} \quad . \quad (38)$$

While proposition 2 holds in the case $p \neq q$, deriving the closed-subset is not possible in the case $p=q$ since the total probability of one will be split over almost all states in a manner that does not clearly privilege some dominant states over the remaining states whose steady-state probabilities tend to zero asymptotically. Despite this observation, the following proposition allows to derive the asymptotic OP and APD in the case $p=q$ while bypassing the tedious evaluation of the steady-state probabilities.

Proposition *3:* Consider the partitioning of the state space into the three sets $\mathcal{I}^{(0)}=\mathcal{L}\times\mathcal{L}$, $\mathcal{I}^{(1)}=\mathcal{L}\times\bar{\mathcal{L}}\cup\bar{\mathcal{L}}\times\mathcal{L}$ and $\mathcal{I}^{(2)}=\bar{\mathcal{L}}\times\bar{\mathcal{L}}$ where $\mathcal{L}=\{0,L\}$ and $\bar{\mathcal{L}}=\{1,\ldots,L-1\}$. For $P_M \gg 1$ and $p=q$:

$$\begin{cases} \pi_{l_1,l_2}=0, & (l_1,l_2)\in\mathcal{I}^{(0)}; \\ \pi_{l_1,l_2}\propto p, & (l_1,l_2)\in\mathcal{I}^{(1)}; \\ \pi_{l_1,l_2}\propto c, & (l_1,l_2)\in\mathcal{I}^{(2)}. \end{cases} \quad (39)$$

implying that:

$$P_{out} \propto p^2q^2 = p^4 \quad ; \quad APD = L \;\; \text{for} \;\; p=q, \quad (40)$$

where $x \propto y$ means that x is proportional to y and c is a constant in (39).

Proof: The proof is provided in Appendix C. ■

The analysis presented in Section III highlights two limitations of the SR scheme. On one hand, increasing the buffer size to reduce the OP will result in increasing the APD implying an inherent tradeoff between the OP and APD levels. On the other hand, the diversity order is significantly improved only with infinite buffer sizes where this choice is not only impractical but it also incurs unbounded delays in the system. These limitations are alleviated by the proposed ISR scheme. In fact, (37) and (40) show that the ISR scheme achieves advantageously small OP levels will finite buffer sizes. As such, unlike the SR scheme, there is no need to increase the buffer size with the ISR protocol which keeps the APD at small and bounded levels while concurrently enhancing the OP performance. In a more detailed manner, for finite buffer sizes,

the OP in (37) and (40) scales asymptotically as $p_{\text{max}}^4 + p^2q^2$ or p^4 where these quantities are several orders of magnitude smaller than the asymptotic value of pq or p_{min}^2 that can be achieved by the SR scheme. Moreover, unlike the SR scheme, the proposed ISR scheme is capable of enhancing the diversity order compared to buffer-free systems while deploying buffers of finite size. In order to realize these much desired diversity gains, the SR scheme must deploy infinite buffer sizes which entails impractical infinite delays. On the other hand, the ISR scheme achieves such gains while keeping the delay bounded at 2 following from (38) and (40) since a finite buffer size of $L = 2$ is sufficient for extracting the full capabilities of the BA network.

In what follows, we compare the presented MC analysis with that of [12], [13]. It is worth highlighting that the dynamics of the buffers in FD FSO systems are more complicated compared to HD RF systems where only one node can transmit in the network. This results in a highly connected MC where a state can be reached from a larger number of other states. For example, transitions of the form $(l_1, l_2) \rightarrow (l_1 + 1, l_2 - 1)$ and $(l_1, l_2) \rightarrow (l_1 - 1, l_2 + 1)$ (as in (18) and (32)) were not possible in [12], [13]. The modified buffer dynamics in FSO networks result in a more involved asymptotic analysis as compared to [12], [13] for the following reasons. (i): In this work, the presented asymptotic analysis varied substantially for the three cases $p < q$, $p > q$ and $p = q$. This entailed three variants of the asymptotic analysis to cover these cases unlike [12], [13] where the reported steady-state probabilities, OP and APD do not vary for the above three cases. (ii): While the asymptotic analysis in [12], [13] as well as the asymptotic analysis of the SR scheme and the ISR scheme (for $p \neq q$) revolved around identifying a closed-subset of dominant states, this type of formulation was not possible for the ISR scheme with $p = q$. For this scenario, the asymptotic OP and APD expressions were derived in an alternative way by determining conditions for which the seven-variable balance equation in (43) holds in the asymptotic regime. (iii): For the scenarios where the closed-subset formulation holds, this formulation is judged to be more challenging in this paper as compared to [12], [13] since the closed-subset contains a larger number of highly connected states. As such, identifying this subset is challenging in the first place and the solution of the approximate balance equations is more involved. For example, in [12], the closed-subset contained only 4 states where each state in this subset was connected to only 2 other states in the asymptotic regime. The analysis of the single-relay two-way scheme in [13] revolved around a closed-subset of 9 states where each state was connected to up to 3 other states asymptotically. On the other hand, the analysis of the SR scheme in this paper was particulary complicated since the closed-subset contained $3L + 1$ states where this number increases rapidly with the buffer size L. In this scenario, each state in the closed-subset was connected to 3 other states in the asymptotic regime. Finally, for the proposed ISR scheme with $p \neq q$, despite the relatively small number of states in the closed-subset (that is equal to 7), the high connectivity of the MC rendered the asymptotic analysis more challenging since a state of the closed-subset can be connected to up to 6 other states.

Since the SR scheme revolves around the selection of the strongest links, then the practical implementation of this scheme necessitates the acquisition of the exact values of the path gains. This entails the implementation of rather involved channel estimation techniques based on the transmission of long sequences of pilot symbols. In this case, each relay needs to feedback to the central node S $\lceil \log_2(M^2) \rceil$ bits of CSI signaling information pertaining to this relay's links with S and D where M stands for the number of levels needed to quantize the continuous-value path gain. On the other hand, while the theoretical performance analysis of the ISR scheme revolves around the outage probabilities p and q, the practical implementation of this scheme requires determining simply whether the links are in outage or not. This can be realized in a simple manner by sending short sequences of pilot symbols and observing whether these symbols were correctly decoded or not without the need of estimating the exact values of the path gains. As such, only two CSI signaling bits need to be communicated by each relay R_k informing the central node on whether the S-R_k and R_k-D links are in outage or not. Note that M must be very large if the channel gains are to be acquired with a satisfactory level of accuracy. Therefore, the deployment of the proposed ISR scheme alleviates the CSI acquisition requirements and limits the CSI-related signaling overhead as compared to the SR scheme.

Based on the above discussion, ISR outperforms SR in terms of the OP and APD performance while requiring a limited signaling overhead and deploying practical finite-size buffers of size two. The performance of the superior ISR scheme can be further improved by optimizing the placement of the relays. This optimization is particularly relevant to cooperative FSO networks with dedicated infrastructure where the relays are deployed with the sole objective of assisting S in its communication with D. As will be highlighted in Section V, adequately placing the relays results in significant reductions of the OP while keeping the asymptotic APD fixed at the minimum value of 2 for $L = 2$ following from (38) and (40). From (37) and (40), $P_{out} = p_{\text{max}}^4 + p^2q^2 \geq [\max\{p, q\}]^4$ for $p \neq q$ while $P_{out} = p^2q^2 = p^4$ for $p = q$. As such, since $p \leq \max\{p, q\}$, then the choice $p = q$ results in the minimum OP value. This result is comparable with buffer-free relaying networks where the outage probability $(p + q - pq)^2 \approx (p + q)^2$ is minimized for $p = q$. If both S-R and R-D hops are identically distributed, the relation $p = q$ implies that $d_1 = d_2$ highlighting that the relays must be placed in the bisecting plane of [S D]. Since the outage probability decreases with the link distance, then fixing $d_1 = d_2 = \frac{d_{\text{SD}}}{2}$ results in the best possible performance. Note that regions in the vicinity of the midpoint of [S D] might not be feasible (because of the presence of obstacles that block the LoS FSO links, for example). In this case, the smallest distance $d_1 = d_2$ that results in a feasible placement constitutes the best option. On the other hand, for non-identically distributed channels, the relation $p = q$ does not necessarily imply that $d_1 = d_2$. In this case, since the outage probabilities scale as $P_M^{-\delta_n} = P_M^{-\min\{\beta_n, \xi_n^2\}}$ in the asymptotic regime, then

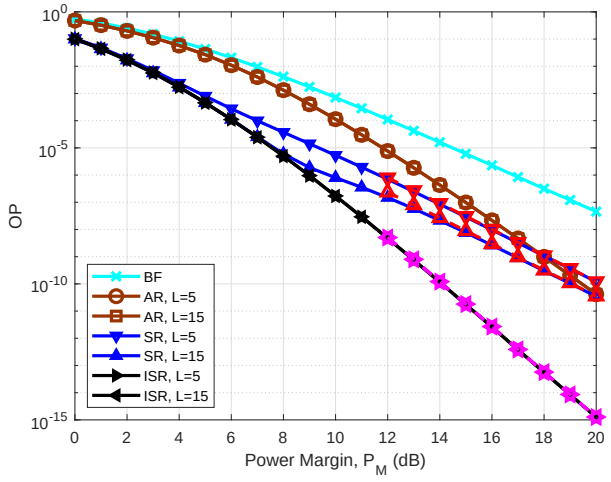

Fig. 2. OP for $d_1 = 2$ km and $d_2 = 1.75$ km. Solid and dashed lines correspond to the exact and asymptotic values, respectively.

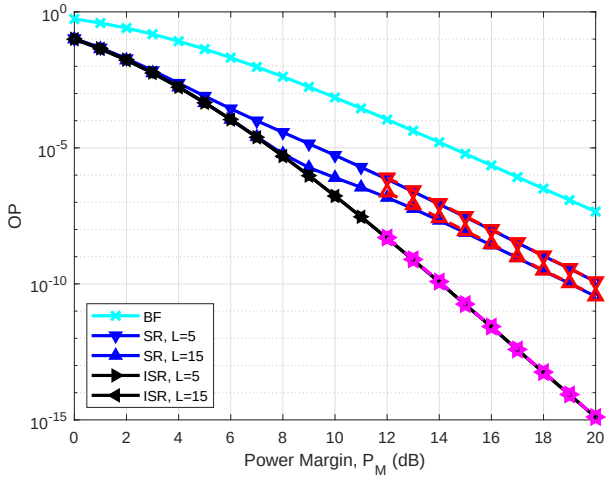

Fig. 4. OP for $d_1 = 1.75$ km and $d_2 = 2$ km. Solid and dashed lines correspond to the exact and asymptotic values, respectively.

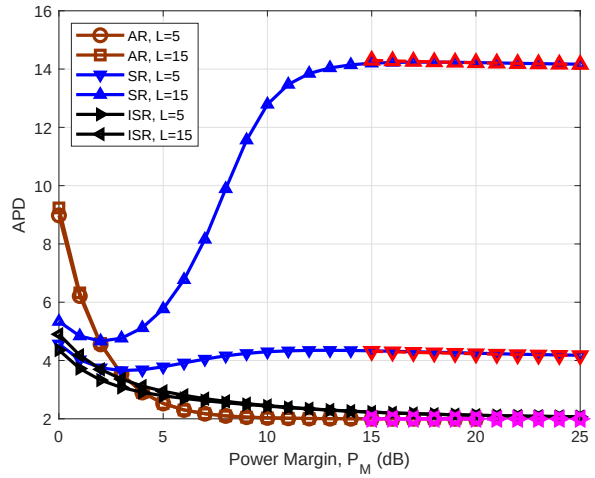

Fig. 3. APD for $d_1 = 2$ km and $d_2 = 1.75$ km. Solid and dashed lines correspond to the exact and asymptotic values, respectively.

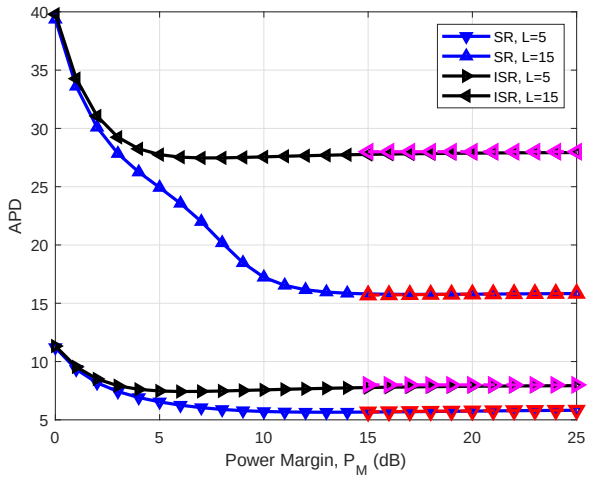

Fig. 5. APD for $d_1 = 1.75$ km and $d_2 = 2$ km. Solid and dashed lines correspond to the exact and asymptotic values, respectively.

the optimal relay placement can be obtained by solving the equation $\min\{\beta_1, \xi_1^2\} = \min\{\beta_2, \xi_2^2\}$ where the coefficients β_1 and β_2 depend nonlinearly on the distances d_1 and d_2 through the Rytov variance following from (3).

V. Numerical Results

We next present some numerical results that support the reported theoretical findings. The refractive index structure constant and the attenuation constant are set to $C_n^2 = 1.7 \times 10^{-14}$ m$^{-2/3}$ and $\sigma = 0.44$ dB/km, respectively. The receiver radius (a), beam waist (ω_z) and pointing error displacement standard deviation (σ_s) are assumed to be the same for all nodes with $\sigma_s/a = 3$ and $\omega_z/a = 10$. S and D are separated by a fixed distance of $d_{\text{SD}} = 3$ km while the distances d_1 and d_2 of the two hops are varied. Three simulation scenarios are considered. Scenario-1: $(d_1, d_2) = (2, 1.75)$ km resulting in $p > q$ where the OP and APD curves are shown in Fig. 2 and Fig. 3, respectively. Scenario-2: $(d_1, d_2) = (1.75, 2)$ km ($p < q$) with the results shown in Fig. 4 and Fig. 5. Scenario-3: we consider a symmetrical network in Fig. 6 and Fig. 7 with $d_1 = d_2 = 2$ km resulting in $p = q$. The numerical results were obtained by running ten million Monte Carlo simulations that yielded accurate OP and APD results for practical values of the SNR. The simulations demonstrated an extremely close match between the numerical results and the analytical results provided in Section III and Section IV. As such, the numerical results were not plotted in the subsequent figures for the sake of clarity of these figures. Note that the simulation results were used to check the accuracy of the analytical results only for small-to-average values of P_M whereas the OP and APD curves provided in figures 2-10 correspond to the analytical results that hold for all values of P_M.

Results in Fig. 2, Fig. 4 and Fig. 6 highlight on the accuracy of the asymptotic OP expressions derived in (25), (37) and (40) for the SR and ISR algorithms under the three considered scenarios. Similarly, results in Fig. 3, Fig. 5 and Fig. 7

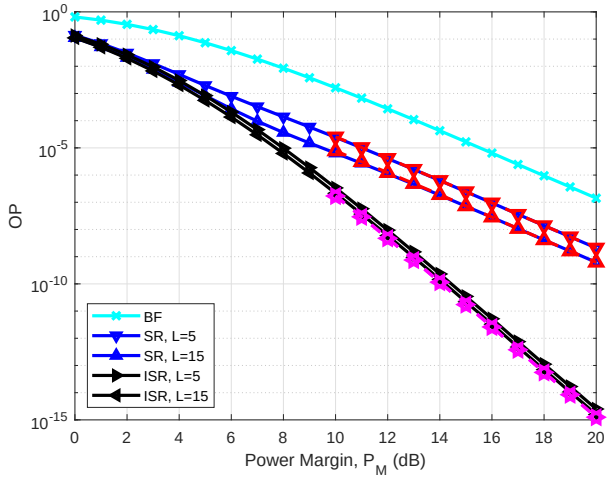

Fig. 6. OP for $d_1 = d_2 = 2$ km. Solid and dashed lines correspond to the exact and asymptotic values, respectively.

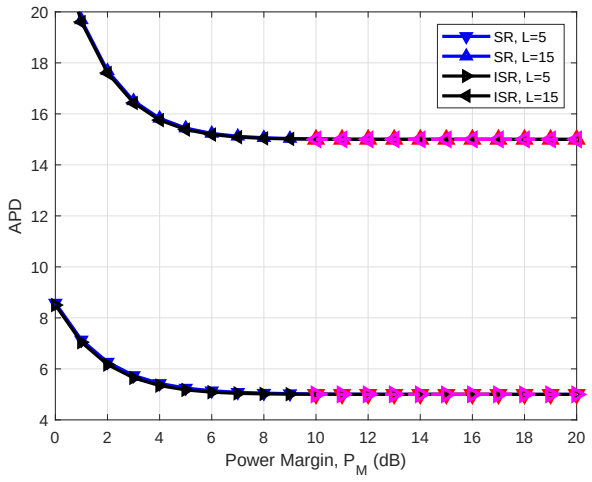

Fig. 7. APD for $d_1 = d_2 = 2$ km. Solid and dashed lines correspond to the exact and asymptotic values, respectively.

demonstrate the usefulness of the simple expressions in (27), (38) and (40) for predicting the asymptotic APD performance. Results in Fig. 2, Fig. 4 and Fig. 6 show the OP improvements that can be achieved by the ISR scheme under all scenarios. These figures also demonstrate the diversity gains reaped by the ISR protocol and the limited diversity orders achieved by the existing SR scheme with finite buffer sizes. As highlighted in Section III, the OP of the SR scheme decreases with L unlike the proposed ISR scheme where the buffer size L does not affect the OP performance. This highlights on the main advantage of the ISR scheme that is capable of achieving significant OP and diversity gains while deploying buffers with finite size that avoid the excessive queuing of the packets, thus, positively impacting the delay. As a benchmark, Fig. 2, Fig. 4 and Fig. 6 include the performance of buffer-free (BF) systems whose OP is given by $[p+q-pq]^2$. On the other hand, since the relays are not equipped with buffers in BF systems and since the full-duplex FSO relays can simultaneously transmit and receive, then the delay in the delivery of the packets corresponds only to the processing delays at the relays where these delays can be ignored compared to the queuing delays in BA systems. Results highlight on the huge OP gains that can be reaped by equipping the relays with buffers. For example, for symmetrical networks in Fig. 6, the proposed BA ISR scheme with a buffer size of five outperforms BF systems by 7.5 dB at an OP of 10^{-5}.

Fig. 2 and Fig. 3 also include the OP and APD curves, respectively, of the BA FSO all-active-relaying scheme (AR) proposed in [4]. This scheme is based on activating all available S-R and R-D links in the network while avoiding the storage of redundant replicas of the information packets in the relays' buffers. This was achieved by retaining the received packet in the buffer with the smallest length while dropping the replicas of this packet from the remaining buffers in an attempt to realize load balancing [4]. Results in Fig. 2 show that the AR scheme suffers from high OP values. In this context, the proposed ISR scheme significantly outperforms the existing AR scheme by around 4.5 dB at an OP value of 10^{-5}. Results in Fig. 3 demonstrate an appealing APD performance of the AR scheme that is comparable to that of the ISR scheme in the high-SNR range. While the APD values of the AR scheme are slightly better for the mid-SNR range, the APD gains of the ISR scheme are particularly visible in the low-SNR range. As a conclusion, the highly poor OP performance of the AR scheme overwhelms its satisfactory APD performance thus highlighting on the superiority of the proposed ISR protocol.

From Fig. 3, the OP improvements of ISR with respect to SR are associated with a reduction in the delay when $p > q$. In this case, ISR achieves the smallest reported asymptotic APD value of 2 regardless of the buffer size. In fact, since $p > q$, the relays' buffers are not congested since the departure rate (along the R-D hop) exceeds the arrival rate (along the S-R hop) which positively contributes to reducing the queuing delays. In the case $p < q$, results in Fig. 5 show that the OP improvements come at the expense of doubling the asymptotic APD as highlighted in (27) and (38). Finally, for $p = q$, ISR achieves the highest diversity gain compared to SR as highlighted in Fig. 6 while manifesting a comparable APD performance as shown in Fig. 7.

It is worth highlighting that the analytical framework presented in this paper revolves mainly around the outage probabilities p and q regardless of how these probabilities are obtained from the underlying weather conditions. In order to demonstrate the validity of the obtained results under different weather conditions, Fig. 8 and Fig. 9 show the OP and APD performance for $L = 10$, $d_{\text{SD}} = 1$ km and $d_1 = d_2 = 750$ m. We consider the "clear air" conditions with $C_n^2 = 1.7\times10^{-14}$ $\text{m}^{-2/3}$ and $\sigma = 0.44$ dB/km and the "light fog" conditions with $C_n^2 = 3\times10^{-15}$ $\text{m}^{-2/3}$ and $\sigma = 20$ dB/km where these values constitute the typical values used in the literature [30]. While identically distributed channels were considered so far where all links are subject to the same weather impairments, Fig. 8 and Fig. 9 also consider the case of non-identical channels where the S-R links experience "light fog" while the statistics of the R-D links are determined assuming the

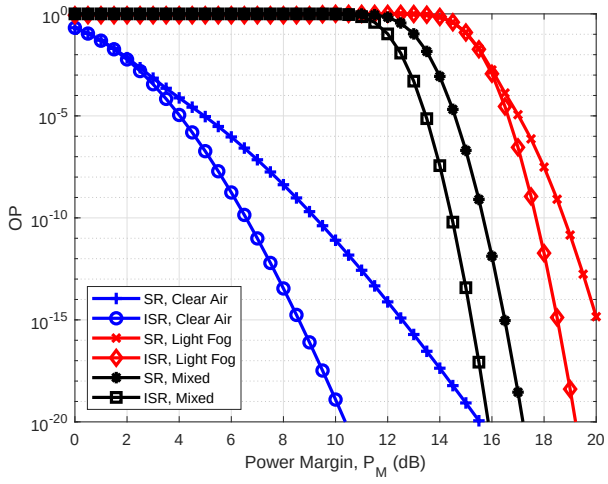

Fig. 8. OP for $L = 10$, $d_{\text{SD}} = 1$ km and $d_1 = d_2 = 750$ m under different weather conditions.

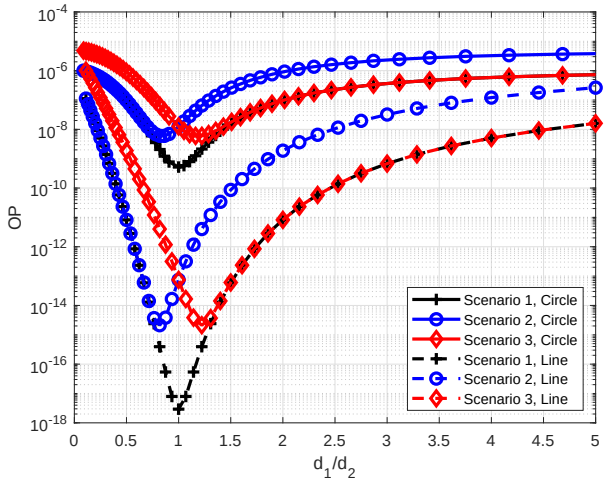

Fig. 10. OP of the ISR scheme for $P_M = 15$ dB, $L = 2$ and $d_{\text{SD}} = 3$ km.

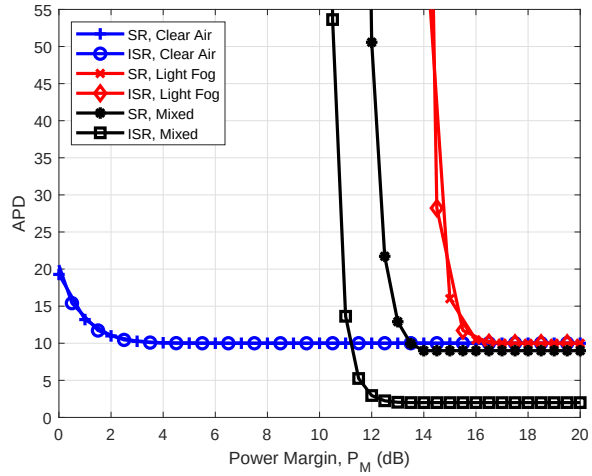

Fig. 9. APD for $L = 10$, $d_{\text{SD}} = 1$ km and $d_1 = d_2 = 750$ m under different weather conditions.

"clear air" conditions. This last scenario is referred to as the "mixed" setup in Fig. 8 and Fig. 9. This scenario is introduced for the sake of demonstrating the superiority of the proposed relaying scheme even when the turbulence and attenuation parameters are not the same for all links even though this scenario is not very probable in practice given the proximity of the nodes in the FSO network rendering all links subject to comparable weather effects. Results in Fig. 8 highlight on the improved OP levels that can be achieved by the proposed ISR scheme under the three considered "clear air", "light fog" and "mixed" weather conditions. Note that the turbulence is weaker with "light fog" resulting in steeper OP curves for large values of P_M whereas the excessive attenuation incurs significant OP degradations for small values of P_M. Results in Fig. 9 demonstrate the accuracy of the derived asymptotic APD expressions. Note that, for the "clear air" and "light fog" scenarios, the choice $d_1 = d_2$ implies that $p = q$ resulting in an asymptotic APD value of L for both the SR and ISR schemes following from (27) and (40). For the "mixed" setup, $p > q$ following from the more severe weather conditions along the S-R hop implying an advantageous asymptotic APD value of 2 for the ISR scheme following from (38) and an asymptotic APD value of $L - 1$ for the SR scheme following from (27). For the "light fog" and "mixed" conditions, the low-SNR delays are excessively large following from the increased unavailability of the FSO links. This issue can be solved by implementing hybrid RF/FSO connections where, for the RF links, any one of the existing RF BA half-duplex schemes can be implemented [8], [10], [11].

The impact of the placement of the relays on the OP of the ISR scheme is verified in Fig. 10 for $P_M = 15$ dB, $L = 2$ and $d_{\text{SD}} = 3$ km. The three following scenarios are considered. Scenario 1: identical channels with $C_n^2 = 1.7 \times 10^{-14}$ m$^{-2/3}$ for both hops. Scenario 2: non-identical channels with $C_n^2 = 3 \times 10^{-14}$ m$^{-2/3}$ along the S-R hop and $C_n^2 = 1.7 \times 10^{-14}$ m$^{-2/3}$ along the R-D hop. Scenario 3: non-identical channels with $C_n^2 = 1.7 \times 10^{-14}$ m$^{-2/3}$ along the S-R hop and $C_n^2 = 3 \times 10^{-14}$ m$^{-2/3}$ along the R-D hop. The relays' positions are varied either along the circle of diameter [S D] (such that $d_1^2 + d_2^2 = d_{\text{SD}}^2$) or along the line [S D] (such that $d_1 + d_2 = d_{\text{SD}}$). Results show that varying the positions along the line results in smaller OPs since the links will become shorter. For identical channels, the OP is minimized for $d_1 = d_2$. For non-identical channels, the optimal value of d_1/d_2 matches the solution of the equation $\min\{\beta_1, \xi_1^2\} = \min\{\beta_2, \xi_2^2\}$. To satisfy this relation, the relays must be moved closer to S when the turbulence is stronger along the S-R hop (scenario 2) while the relays must be moved closer to D when the turbulence is stronger along the R-D hop (scenario 3).

VI. Conclusion

We provided a theoretical performance analysis of the existing FSO SR protocol and we proposed an improvement to this protocol that is better tailored to realistic systems deploying finite size buffers. The theoretical evaluation highlighted that the proposed scheme is capable of enhancing the diversity

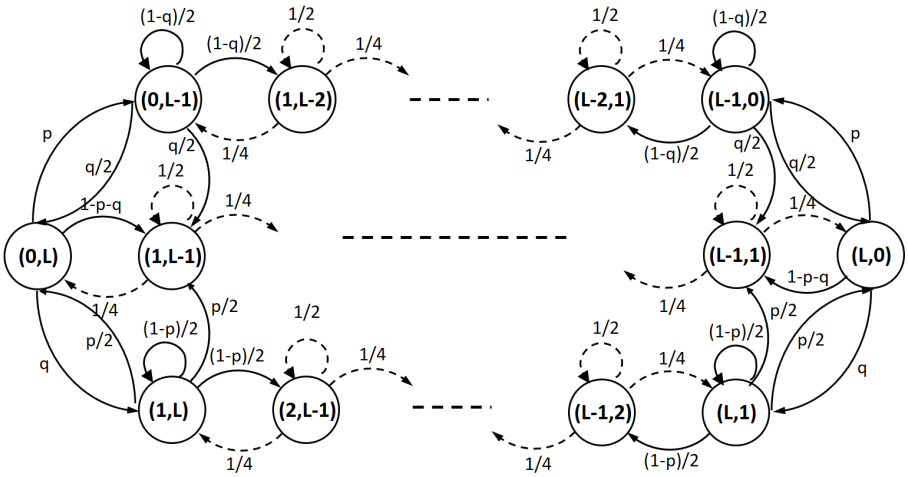

Fig. 11. The closed-subset $\mathcal{S}$ and the corresponding transitions in the asymptotic regime.

order without the need of implementing buffers of infinite size that incur infinite delays. While the derived closed-form asymptotic performance metrics hold for two-relays networks, future work must consider the extension of the performance analysis to networks with any number of relays. Increasing the number of relays is expected to improve the availability of the network and reduce the delays.

Appendix A

We first prove that $t_{(l_1,l_2),(l_1',l_2')} \to 0$ for $(l_1,l_2) \in \mathcal{S}$ and $(l_1',l_2') \notin \mathcal{S}$. The transitions in (15) and (18) do not yield to states outside $\mathcal{S}$ since $l_1'+l_2' = l_1+l_2$ for all $(l_1',l_2') \in \{(l_1,l_2),(l_1+1,l_2-1),(l_1-1,l_2+1)\}$ and, therefore, $(l_1',l_2') \in \mathcal{S}$ whenever $(l_1,l_2) \in \mathcal{S}$ following from (19). Consequently, in what follows we need to consider only the transitions in (16) and (17).

The set $\mathcal{S}$ can be further partitioned as $\mathcal{S} = \mathcal{S}' \cup \mathcal{S}''$ where $\mathcal{S}' = \{(l_1,l_2) \mid l_1 \neq 0, L \ ; \ l_2 \neq 0, L\}$ and $\mathcal{S}'' = \{(0,L-1),(L-1,0),(0,L),(L,0),(1,L),(L,1)\}$. For the elements of $\mathcal{S}'$, the transition probabilities in (16) and (17) tend to q^2 and p^2 asymptotically, respectively, since $\phi = \psi = 2$ in this case. As such, the corresponding transitions can be ignored for $p \ll 1$ and $q \ll 1$. We next consider the elements of $\mathcal{S}''$. For the states $(0,L)$ and $(L,0)$, the transitions in (16)-(17) yield to the states $\{(1,L),(0,L-1)\}$ and $\{(L,1),(L-1,0)\}$, respectively, where all of these four states belong to $\mathcal{S}$. For the states $(0,L-1)$ and $(L-1,0)$, the transitions in (16) are confined in $\mathcal{S}$. On the other hand, the transition probabilities in (17) are proportional to p^2 since $(\phi,\psi) = (2,1)$ in this case implying that these transitions that yield to states outside $\mathcal{S}$ can be ignored asymptotically. Finally, for the states $(1,L)$ and $(L,1)$, $(\phi,\psi) = (1,2)$ where the transitions in (17) are confined in $\mathcal{S}$ while the transitions in (16) that might yield outside $\mathcal{S}$ can be ignored since they occur with a probability that is proportional to q^2.

The closed-subset $\mathcal{S}$ is shown in Fig. 11 where the high order probabilities p^2, q^2 and pq were ignored. From Fig. 11, the balance equation at a state (l_1,l_2) of $\mathcal{S}'$ can be written as:

$$\pi_{l_1,l_2} = \frac{1}{2}\pi_{l_1,l_2} + \alpha\pi_{l_1-1,l_2+1} + \beta\pi_{l_1+1,l_2-1}. \tag{41}$$

(i): For $l_1+l_2 = L-1$, $\alpha = \frac{1}{4}\delta_{l_1\neq 1} + \frac{1}{2}\delta_{l_1=1}$ and $\beta = \frac{1}{4}\delta_{l_2\neq 1} + \frac{1}{2}\delta_{l_2=1}$ where $\delta_s = 1$ if the statement s is true and $\delta_s = 0$ otherwise while the approximation $\frac{1-q}{2} \approx \frac{1}{2}$ was used in the expressions of α and β. As such, the solution provided in (20) satisfies (41) for $l_1+l_2 = L-1$. (ii): For $l_1+l_2 = L$, $\alpha = \frac{1}{4}\delta_{l_1\neq 1} + \delta_{l_1=1}$ and $\beta = \frac{1}{4}\delta_{l_2\neq 1} + \delta_{l_2=1}$ (where $1-p-q \approx 1$) implying that the solution in (21) satisfies (41) in this case. (iii): For $l_1+l_2 = L+1$, $\alpha = \frac{1}{4}\delta_{l_1\neq 2} + \frac{1}{2}\delta_{l_1=2}$ and $\beta = \frac{1}{4}\delta_{l_2\neq 2} + \frac{1}{2}\delta_{l_2=2}$ (where $\frac{1-p}{2} \approx \frac{1}{2}$) demonstrating that the recursive solution of (41) is as provided in (22).

Next, we relate the probabilities μ_1, μ_2 and μ_3 in (20)-(22) to each other by manipulating the balance equations at states of $\mathcal{S}''$. Adding up the balance equations at the states $(1,L-1)$ and $(0,L)$ then replacing in the balance equations at the states $(0,L-1)$ and $(0,L)$ results in the relations $q\mu_1 = p\mu_2$ and $p\mu_3 = q\mu_2$. As such, for $p = q$, $\mu_1 = \mu_2 = \mu_3$ as highlighted in (23). For $p > q$, $\mu_1 = \frac{p}{q}\mu_2$ while the probability $\mu_3 = \frac{q}{p}\mu_2$ can be ignored for $P_M \gg 1$. In fact, both p and q are decreasing functions of P_M implying that the gap between these probabilities will increase as P_M increases implying that the ratio q/p can be ignored in this case where the scintillation and/or pointing errors are more severe along the first hop. Similarly, for $p < q$, the probability $\mu_3 = \frac{q}{p}\mu_2$ must be included in the calculations while the probability $\mu_1 = \frac{p}{q}\mu_2$ can be ignored.

Since we have proven that the set $\mathcal{S}$ is closed, then $\sum_{(l_1,l_2)\in\mathcal{S}} \pi_{l_1,l_2} \to 1$. Following from (20)-(22), this results in:

$$2\mu_1 + 2\mu_1(L-2) + 2\mu_2 + 4\mu_2(L-1) + 2\mu_3 + 2\mu_3(L-2) = 1. \tag{42}$$

Finally, replacing μ_1 and μ_3 by their values as a function of μ_2 in (42) yields to the solution provided in (23).

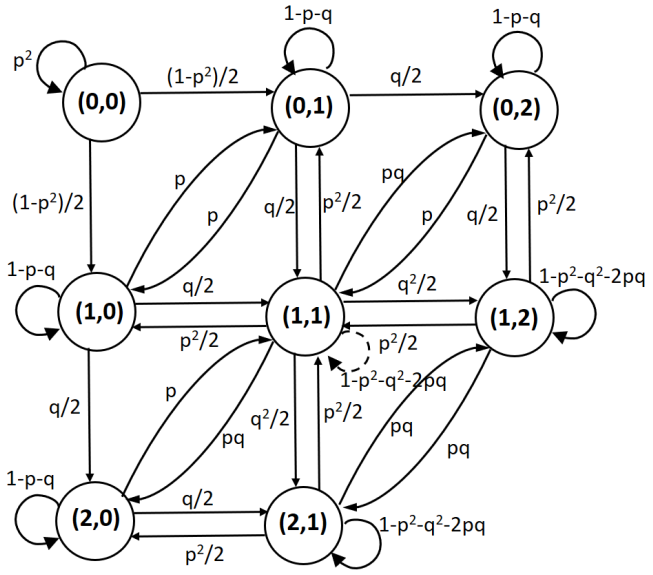

Fig. 12. The closed-subset $\mathcal{S}_0$ for the ISR scheme with $p > q$.

APPENDIX B

We first consider the case $p > q$ and prove that the set $\mathcal{S}_0$ in (33) is closed. From (29)-(32), the transitions from the states $(0,0)$, $(0,1)$ and $(1,0)$ are confined in $\mathcal{S}_0$. Moreover, the transitions from the states $(1,2)$ and $(2,1)$ to the states outside $\mathcal{S}_0$ occur with probabilities $\frac{1}{2}p^2$, $\frac{1}{2}q^2$ and pq and, consequently, can be neglected. Finally, from the states $(0,2)$ and $(2,0)$, we can exit $\mathcal{S}_0$ with the probability $\frac{1}{2}q$ that tends to zero since q is neglected compared to p in this case where $p > q$. Therefore, the set $\mathcal{S}_0$, shown in Fig. 12, is closed.

From Fig. 12, the probability of exiting the state $(0,0)$ is $1-p^2 \approx 1$ and, hence, $\pi_{0,0} = 0$. From the symmetry of the transitions in Fig. 12, we can deduce that $\pi_{0,1} = \pi_{1,0} \triangleq \nu_2$, $\pi_{0,2} = \pi_{2,0} \triangleq \nu_3$ and $\pi_{1,2} = \pi_{2,1} \triangleq \nu_4$. Next, we will relate the probabilities ν_2, ν_3 and ν_4 to the probability $\pi_{1,1} \triangleq \nu_1$. The balance equation at $(0,1)$ can be written as $(p+q)\nu_2 = p\nu_2 + \frac{1}{2}p^2\nu_1$ implying that $\nu_2 = \frac{p^2}{2q}\nu_1$. The balance equations at $(1,1)$ and $(1,2)$ are given by $(p^2+q^2+2pq)\nu_1 = q\nu_2 + 2p\nu_3 + p^2\nu_4$ and $(p^2+q^2+2pq)\nu_4 = \frac{q^2}{2}\nu_1 + \frac{q}{2}\nu_3 + pq\nu_4$, respectively. Replacing ν_2 by its value in these equations and solving for ν_3 and ν_4 results in $\nu_3 = \frac{p}{4}\nu_1$ and $\nu_4 = \frac{q}{8p}\nu_1$. Since the MC is in $\mathcal{S}_0$ with a probability that tends to one asymptotically, then $\nu_1 + 2\nu_2 + 2\nu_3 + 2\nu_4 = 1$. Replacing ν_2, ν_3 and ν_4 by their values in the last equation and solving for ν_1 results in the solution provided in (35).

A similar proof holds in the case $p < q$ by interchanging the probabilities p and q and by replacing the states (l_1, l_2) of $\mathcal{S}_0$ by the states $(L-l_1, L-l_2)$.

APPENDIX C

From (30)-(32), the probabilities of exiting the states $(0,0)$, $(0,L)$, $(L,0)$ and (L,L) are $1-p^2$, 1, 1 and $1-q^2$, respectively, where all these probabilities tend to one asymptotically. As such, $\pi_{l_1,l_2} = 0$ for $(l_1,l_2) \in \mathcal{I}^{(0)}$.

For $p = q$, the balance equation at any state $(l_1,l_2) \in \mathcal{I}^{(2)}$ can be written as the summation of six terms as follows:

$$4p^2\pi_{l_1,l_2} = \pi_{l_1+1,l_2-1}\chi_1 + \pi_{l_1-1,l_2+1}\chi_2 + \frac{p}{2}\pi_{l_1-1,l_2}\left[\delta_{l_1=1} + p\delta_{l_1\neq 1}\right] + \frac{p}{2}\pi_{l_1+1,l_2}\left[\delta_{l_1=L-1} + p\delta_{l_1\neq L-1}\right] + \frac{p}{2}\pi_{l_1,l_2-1}\left[\delta_{l_2=1} + p\delta_{l_2\neq 1}\right] + \frac{p}{2}\pi_{l_1,l_2+1}\left[\delta_{l_2=L-1} + p\delta_{l_2\neq L-1}\right], \quad (43)$$

where:

$$\chi_1 = p(\delta_{l_1\neq L-1}\delta_{l_2=1} + \delta_{l_1=L-1}\delta_{l_2\neq 1}) + p^2\delta_{l_1\neq L-1}\delta_{l_2\neq 1}$$
$$\chi_2 = p(\delta_{l_1\neq 1}\delta_{l_2=L-1} + \delta_{l_1=1}\delta_{l_2\neq L-1}) + p^2\delta_{l_1\neq 1}\delta_{l_2\neq L-1}. \quad (44)$$

For the equality in (43) to hold for all values of p, the following conditions must hold. (i): From the third term in the summation, $\pi_{l_1-1,l_2} \propto c$ for $l_1 \neq 1$ and $\pi_{l_1-1,l_2} \propto p$ for $l_1 = 1$ implying that $\pi_{l_1,l_2} \propto c$ for $l_1 \neq 0$ and $\pi_{l_1,l_2} \propto p$ for $l_1 = 0$ where c is a constant. (ii): From the fourth term in the summation, $\pi_{l_1+1,l_2} \propto c$ for $l_1 \neq L-1$ and $\pi_{l_1+1,l_2} \propto p$ for $l_1 = L-1$ implying that $\pi_{l_1,l_2} \propto c$ for $l_1 \neq L$ and $\pi_{l_1,l_2} \propto p$ for $l_1 = L$. (iii): Similarly, from the fifth and sixth terms in the summation, we can deduce that $\pi_{l_1,l_2} \propto c$ for $l_2 \neq 0$ and $\pi_{l_1,l_2} \propto p$ for $l_2 = 0$ and $\pi_{l_1,l_2} \propto c$ for $l_2 \neq L$ and $\pi_{l_1,l_2} \propto p$ for $l_2 = L$. The above results imply that $\pi_{l_1,l_2} \propto p$ for $(l_1,l_2) \in \mathcal{I}^{(1)}$ and $\pi_{l_1,l_2} \propto c$ for $(l_1,l_2) \in \mathcal{I}^{(2)}$. This conclusion also ensures that the left-hand-side of (43) and the first two terms in the summation to the right-hand-side of (43) are all proportional to p^2 thus completing the proof of (39).

Following from (39), the OP in (11) can be written as:

$$P_{out} = \sum_{(l_1,l_2)\in\mathcal{I}^{(1)}} \underbrace{\pi_{l_1,l_2}}_{\propto p} p^3 + \sum_{(l_1,l_2)\in\mathcal{I}^{(2)}} \underbrace{\pi_{l_1,l_2}}_{\propto c} p^4, \quad (45)$$

since for $(l_1,l_2) \in \mathcal{I}^{(1)}$, $(\phi,\psi) \in \{(1,2),(2,1)\}$ implying that $p^\phi q^\psi = p^3$ for $p = q$. Similarly, for $(l_1,l_2) \in \mathcal{I}^{(2)}$, $\phi = \psi = 2$ implying that $p^\phi q^\psi = p^4$. Form (45), it can be concluded that P_{out} is proportional to p^4 as highlighted in (40).

In (43), the probabilities multiplying the terms $\delta_{l_1=1}$ and $\delta_{l_1=L-1}$ are the same. The same holds for the probabilities multiplying $(\delta_{l_1\neq 1}, \delta_{l_1\neq L-1})$, $(\delta_{l_2=1}, \delta_{l_2=L-1})$ and $(\delta_{l_2\neq 1}, \delta_{l_2\neq L-1})$ implying that:

$$\pi_{l_1,l_2} = \pi_{L-l_1,L-l_2} \quad \forall \quad (l_1,l_2) \in \mathcal{I}^{(2)}. \quad (46)$$

The steady-state probabilities of elements of $\mathcal{I}^{(1)}$ are proportional to p and, hence, can be ignored in the evaluation of the asymptotic delay. Therefore, (13) can be written as:

$$\bar{L} \triangleq S_1 + S_2 + S_3 = \sum_{i=1}^{3} \sum_{(l_1,l_2)\in\mathcal{I}_i^{(2)}} \pi_{l_1,l_2}(l_1+l_2), \quad (47)$$

where $\mathcal{I}_1^{(2)}$, $\mathcal{I}_2^{(2)}$ and $\mathcal{I}_3^{(2)}$ contain the elements of $\mathcal{I}^{(2)}$ such that $l_1+l_2 < L$, $l_1+l_2 = L$ and $l_1+l_2 > L$, respectively.

Carrying out the changes of variables $l_1 \to L-l_1$ and $l_2 \to L-l_2$ in S_3 while invoking (46) implies that $S_1 + S_3 = 2L\sum_{(l_1,l_2)\in\mathcal{I}_1^{(2)}} \pi_{l_1,l_2}$. As such, (47) can be written as $\bar{L} = L\left[2\sum_{(l_1,l_2)\in\mathcal{I}_1^{(2)}} \pi_{l_1,l_2} + \sum_{(l_1,l_2)\in\mathcal{I}_2^{(2)}} \pi_{l_1,l_2}\right] = L$ since $\sum_{(l_1,l_2)\in\mathcal{I}_1^{(2)}} \pi_{l_1,l_2} = \sum_{(l_1,l_2)\in\mathcal{I}_3^{(2)}} \pi_{l_1,l_2}$ following from (46)

while the sum of the steady-state probabilities of the elements of $\mathcal{I}^{(2)}$ tends to one asymptotically. Approximating (12) by $\bar{L}$ results in the asymptotic APD expression provided in (40).

REFERENCES

[1] M. A. Khalighi and M. Uysal, "Survey on free space optical communication: A communication theory perspective," *IEEE communications surveys & tutorials*, vol. 16, no. 4, pp. 2231–2258, Nov. 2014.

[2] M. Safari and M. Uysal, "Relay-assisted free-space optical communication," *IEEE Trans. Wireless Commun.*, vol. 7, no. 12, pp. 5441 – 5449, Dec. 2008.

[3] B. Zhu, J. Cheng, M. Alouini, and L. Wu, "Relay placement for FSO multi-hop DF systems with link obstacles and infeasible regions," *IEEE Trans. Wireless Commun.*, vol. 14, no. 9, pp. 5240 – 5250, Sep. 2015.

[4] C. Abou-Rjeily and W. Fawaz, "Buffer-aided relaying protocols for cooperative FSO communications," *IEEE Trans. Wireless Commun.*, vol. 16, no. 12, pp. 8205–8219, Dec. 2017.

[5] ——, "Buffer-aided serial relaying for FSO communications: asymptotic analysis and impact of relay placement," *IEEE Trans. Wireless Commun.*, vol. 17, no. 12, pp. 8299–8313, Dec. 2018.

[6] W. Fawaz, C. Abou-Rjeily, and C. Assi, "UAV-aided cooperation for FSO communication systems," *IEEE Communications Magazine*, vol. 56, no. 1, pp. 70–75, Jan. 2018.

[7] C. Abou-Rjeily and W. Fawaz, "Quality-of-service differentiation in buffer-aided cooperative free space optical communication systems," *IEEE Trans. Wireless Commun.*, vol. PP, no. 99, pp. 1 – 1, Apr. 2021.

[8] I. Krikidis, T. Charalambous, and J. S. Thompson, "Buffer-aided relay selection for cooperative diversity systems without delay constraints," *IEEE Trans. Wireless Commun.*, vol. 11, no. 5, pp. 1957–1967, May 2012.

[9] Z. Tian, Y. Gong, G. Chen, and J. Chambers, "Buffer-aided relay selection with reduced packet delay in cooperative networks," *IEEE Trans. Veh. Technol.*, vol. 66, no. 3, pp. 2567–2575, Mar. 2017.

[10] S. Luo and K. C. Teh, "Buffer state based relay selection for buffer-aided cooperative relaying systems," *IEEE Trans. Wireless Commun.*, vol. 14, no. 10, pp. 5430–5439, Oct. 2015.

[11] B. Manoj, R. K. Mallik, and M. R. Bhatnagar, "Performance analysis of buffer-aided priority-based max-link relay selection in DF cooperative networks," *IEEE Trans. Commun.*, vol. 66, no. 7, pp. 2826–2839, Feb. 2018.

[12] S. El-Zahr and C. Abou-Rjeily, "Threshold based relay selection for buffer-aided cooperative relaying systems," *IEEE Trans. Wireless Commun.*, vol. 22, no. 9, pp. 6210–6223, Sep. 2021.

[13] C. Abou-Rjeily, "Optimal two-way buffer-aided relaying: Achieving the best outage and delay performance with small buffer sizes," *IEEE Trans. Wireless Commun.*, vol. 20, no. 5, pp. 2888–2901, May 2021.

[14] P. Xu, Z. Ding, I. Krikidis, and X. Dai, "Achieving optimal diversity gain in buffer-aided relay networks with small buffer size," *IEEE Trans. Veh. Technol.*, vol. 65, no. 10, pp. 8788–8794, Oct. 2015.

[15] M. M. Razlighi and N. Zlatanov, "Buffer-aided relaying for the two-hop full-duplex relay channel with self-interference," *IEEE Trans. Wireless Commun.*, vol. 17, no. 1, pp. 477–491, Jan. 2018.

[16] A. K. Shukla, B. Manoj, and M. R. Bhatnagar, "Virtual full-duplex relaying in a buffer-aided multi-hop cooperative network," in *2020 Int. Conf. on Signal Process. and Commun. (SPCOM)*. IEEE, 2020, pp. 1–5.

[17] B. Manoj, R. K. Mallik, and M. R. Bhatnagar, "Buffer-aided multi-hop DF cooperative networks: A state-clustering based approach," *IEEE Trans. Commun.*, vol. 64, no. 12, pp. 4997–5010, Dec. 2016.

[18] Z. Tian, G. Chen, Y. Gong, Z. Chen, and J. A. Chambers, "Buffer-aided max-link relay selection in amplify-and-forward cooperative networks," *IEEE Trans. Veh. Technol.*, vol. 64, no. 2, pp. 553–565, Feb. 2015.

[19] T. Charalambous, N. Nomikos, I. Krikidis, D. Vouyioukas, and M. Johansson, "Modeling buffer-aided relay selection in networks with direct transmission capability," *IEEE Commun. Lett.*, vol. 19, no. 4, pp. 649–652, Apr. 2015.

[20] M. Najafi, V. Jamali, and R. Schober, "Optimal relay selection for the parallel hybrid RF/FSO relay channel: Non-buffer-aided and buffer-aided designs," *IEEE Trans. Commun.*, vol. 65, no. 7, pp. 2794–2810, July 2017.

[21] V. Jamali, D. S. Michalopoulos, M. Uysal, and R. Schober, "Link allocation for multiuser systems with hybrid RF/FSO backhaul: Delay-limited and delay-tolerant designs," *IEEE Trans. Wireless Commun.*, vol. 15, no. 5, pp. 3281–3295, May 2016.

[22] Y. F. Al-Eryani, A. M. Salhab, S. A. Zummo, and M.-S. Alouini, "Protocol design and performance analysis of multiuser mixed RF and hybrid FSO/RF relaying with buffers," *OSA J. Opt. Commun. Netw.*, vol. 10, no. 4, pp. 309–321, Apr. 2018.

[23] C. Abou-Rjeily, "Packet unloading strategies for buffer-aided multiuser mixed RF/FSO relaying," *IEEE Wireless Commun. Lett.*, vol. 9, no. 7, pp. 1051–1055, July 2020.

[24] M. Z. Hassan, M. J. Hossain, J. Cheng, and V. C. Leung, "Hybrid RF/FSO backhaul networks with statistical-QoS-aware buffer-aided relaying," *IEEE Trans. Wireless Commun.*, vol. 19, no. 3, pp. 1464–1483, Mar. 2020.

[25] S. Song, Y. Liu, Q. Song, and L. Guo, "Relay selection and link scheduling in cooperative free-space optical backhauling of 5G small cells," in *2017 IEEE/CIC Int. Conf. on Commun. in China (ICCC)*, 2017, pp. 1–6.

[26] J.-Y. Wang, Y. Ma, R.-R. Lu, J.-B. Wanga, M. Lin, and J. Cheng, "Hovering UAV-Based FSO communications: Channel modelling, performance analysis, and parameter optimization," *IEEE J. Select. Areas Commun.*, vol. 39, no. 10, pp. 2946–2959, Oct. 2021.

[27] N. Nomikos, T. Charalambous, I. Krikidis, D. N. Skoutas, D. Vouyioukas, M. Johansson, and C. Skianis, "A survey on buffer-aided relay selection," *IEEE Communications Surveys & Tutorials*, vol. 18, no. 2, pp. 1073–1097, Second Quarter 2016.

[28] A. Farid and S. Hranilovic, "Outage capacity optimization for free-space optical links with pointing errors," *J. Lightwave Technol.*, vol. 25, no. 7, pp. 1702–1710, July 2007.

[29] J. D. C. Little and S. C. Graves, "Little's law," in *International Series in Operations Research & Management Science*, New York, NY, USA: Springer-Verlag, vol. 115, pp. 81–100, 2008.

[30] B. He and R. Schober, "Bit-interleaved coded modulation for hybrid RF/FSO systems," *IEEE Trans. Commun.*, vol. 57, no. 12, pp. 3753–3763, Dec. 2009.